

# Physical and numerical modelling of the inherent variability of shear strength in soil mechanics

Reza Jamshidi Chenari<sup>1a</sup>, Behzad Fatahi<sup>\*2</sup>, Malahat Ghoreishi<sup>1b</sup> and Ali Taleb<sup>1c</sup>

<sup>1</sup>Faculty of Engineering, University of Guilan, Rasht, Guilan, Iran

<sup>2</sup>School of Civil and Environmental Engineering, Faculty of Engineering and Information Technology, University of Technology Sydney (UTS), City Campus PO Box 123 Broadway NSW 2007, Australia

(Received June 27, 2018, Revised December 1, 2018, Accepted December 5, 2018)

**Abstract.** In this study the spatial variability of soils is substantiated physically and numerically by using random field theory. Heterogeneous samples are fabricated by combining nine homogeneous soil clusters that are assumed to be elements of an adopted random field. Homogeneous soils are prepared by mixing different percentages of kaolin and bentonite at water contents equivalent to their respective liquid limits. Comprehensive characteristic laboratory tests were carried out before embarking on direct shear experiments to deduce the basic correlations and properties of nine homogeneous soil clusters that serve to reconstitute the heterogeneous samples. The tests consist of Atterberg limits, and Oedometric and unconfined compression tests. The undrained shear strength of nine soil clusters were measured by the unconfined compression test data, and then correlations were made between the water content and the strength and stiffness of soil samples with different consistency limits. The direct shear strength of heterogeneous samples of different stochastic properties was then evaluated by physical and numerical modelling using FISH code programming in finite difference software of FLAC<sup>3D</sup>. The results of the experimental and stochastic numerical analyses were then compared. The deviation of numerical simulations from direct shear load-displacement profiles taken from different sources were discussed, potential sources of error was introduced and elaborated. This study was primarily to explain the mathematical and physical procedures of sample preparation in stochastic soil mechanics. It can be extended to different problems and applications in geotechnical engineering discipline to take in to account the variability of strength and deformation parameters.

**Keywords:** inherent variability; undrained cohesion; direct shear test; Monte Carlo simulation

## 1. Introduction

The mechanism that governs the formation of natural deposits leads to variability in soil is expressed as uncertainty, but uncertainty in soil stems from its inherent heterogeneity, errors in measurement, statistical error, and uncertainty in its transformation.

Uncertainty affects the bearing capacity of foundations, slope stability, the settlement of foundations, seepage beneath and through earth dams, and site response analysis due to earthquakes. For example, uncertainties in soil properties can impact design of ground improvement using preloading with vertical drains (Azari *et al.* 2014, Parsa-Pajouh *et al.* 2014) or soil cementation (Nguyen and Fatahi 2016; Nguyen *et al.* 2017) or long term settlement of soils considering creep (Let *et al.* 2017, Le and Fatahi 2016). In

slope stability problems the failure surface passes through points with the lowest shear strength, which means the spatial variability of the shear strength parameters can be very important. As foundations settle the spatial variability of the soil beneath the foundation can increase the magnitude of settlement and result in settlements that are higher than the allowable limits. Moreover, the spatial variability of shear resistance parameters can lower the bearing capacity of shallow foundations, which means that an assumption of higher safety factors does not necessarily lead to a safe design.

The effect that random variations of soil properties have on various geotechnical problems has been studied in recent years; for example, Fenton and Griffiths (2003), Popescu *et al.* (2005), Griffiths *et al.* (2006), Al-Bittar and Soubra (2013), Jamshidi Chenari *et al.* (2013), Jamshidi Chenari and Mahgir (2013), and Wang *et al.* (2018) investigated the bearing capacity of shallow foundations on heterogeneous deposits; Hicks and Spencer (2010), Kasama and Zen (2011), GuhaRay and Baidya (2014), Ji and Liao (2014), Jamshidi Chenari and Alaei (2015), Lim *et al.* (2016), and Huang *et al.* (2016), Lombardi *et al.* (2017) studied the stability of heterogeneous earth or rock slopes; Haldar and Babu (2008), Deb and Majee (2014), Lu *et al.* (2016), Shrestha *et al.* (2017), and Jamshidi Chenari *et al.* (2018a) studied the response of vertically and laterally loaded piles in inherently variable undrained clay deposits; Jamshidi

\*Corresponding author, Associate Professor  
E-mail: Behzad.fatahi@uts.edu.au

<sup>a</sup>Associate Professor  
E-mail: Jamshidi\_reza@guilan.ac.ir

<sup>b</sup>M.Sc. Graduate  
E-mail: Malahatgh1993@yahoo.com

<sup>c</sup>M.Sc. Graduate  
E-mail: Seyyedalitaleb@yahoo.com

Chenari and Kamyab Farahbakhsh (2015), and Jamshidi Chenari *et al.* (2018b) used the CPT profile to study the inherent variability of soil parameters and showed excellent examples of non-stationary random fields in geomechanics, and Fenton and Griffiths (2002), Jimenez and Sitar (2009), and Jamshidi Chenari and Oloomi (2011) examined the settlement of foundations on heterogeneous soil deposits. Srivastava and Babu (2011) investigated the deflection and buckling of pipe buried in spatially variable soil. All this research involved finite or discrete element numerical modelling of a spatially variable deposit using random field theory, and then computing the response statistics using Monte Carlo simulations.

The numerical stochastic geotechnical models are difficult to verify experimentally due to the excessive time and cost required to build full-scale field tests. Pioneer researchers Garzón *et al.* (2015) tried to imitate the inherent heterogeneity of natural alluvial deposits physically and in the laboratory; in fact, their current study presents a technique to prepare scaled heterogeneous soil models with predetermined variability in the laboratory. Samples of heterogeneous soil are produced by simulating variability in their liquid limit, reproducing the history of field stresses using an odometer test, and then investigating the load-displacement behavior of the soil via a direct shear test. Preparing heterogeneous samples with a variable liquid limit field will vary their cohesion. This paper offers a new technique for physically realizing inherent variability in the laboratory. A subsequent set of random finite difference method (RFDM) numerical analysis is also provided to show how efficiently the numerical Monte Carlo simulations can reproduce the load-displacement behavior of samples of heterogeneous soil in direct shear test apparatus.

## 2. Physical modelling of soil variability

Garzón *et al.* (2015) presented an example of a two-dimensional physical soil model by using random field theory in the laboratory. In their model, a mesh with equal elements was used to describe the inherent variability of the liquid limit randomly. This study presents the steps needed to construct two-dimensional physical soil models (100 mm × 100 mm) realized from a prescribed random field, and then the inherent variability of the liquid limit random field will be sought. Thus, the soil will be described by a mesh of equally sized elements for which a liquid limit  $LL$  is assigned randomly according to the stochastic properties of the random field. The mean and coefficient of variation of  $LL$  ( $COV_{LL}$ ), and the auto-correlation distance  $\delta$  along with the probability distribution function constitutes the stochastic properties of the liquid limit random field.

### 2.1 Random field generation

Random field theory can be used to model the inherent variability of soil characteristics. Vanmarcke (1977), describes the inherent variability in geomaterials and proposes the random field theory to deal with this variability. Random field theory is the perfect tool for

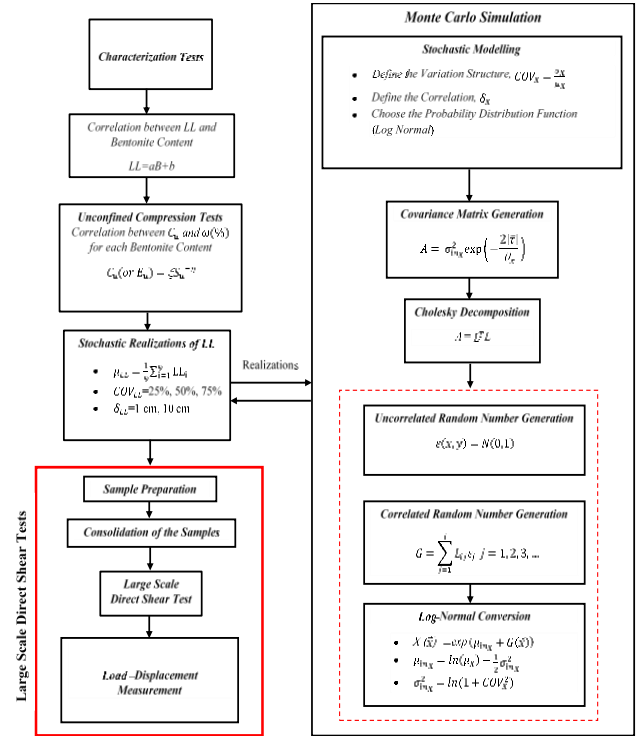


Fig. 1 Flowchart for physical modeling of heterogeneous samples in the laboratory

studying the heterogeneity of material properties in engineering and making it easy to work with uncertainty in engineering problems.

The mean, standard deviation, autocorrelation distance, and the probability distribution function are important parameters for explaining a random field. There are several methods available in literature for generating random fields such as the moving average, co-variance matrix decomposition, the discrete Fourier transform method, and turning-bands (Fenton and Griffiths 2008). In this paper the covariance matrix decomposition was used to reproduce a variable liquid limit (El-Kadi and Williams 2000).

This method applies a covariance matrix decomposition technique to generate 2D auto-correlated liquid limit random field using MATLAB software. Eq. (1) illustrates the auto-correlation function that is decomposed by adopting the Cholesky decomposition technique explained by El-Kadi and Williams (2000) (Eq. (2)).

$$A_{ij} = \sigma_{m_{LL}}^2 \exp\left(-\frac{|d_{ij}^X|}{\delta_X} - \frac{|d_{ij}^Z|}{\delta_Z}\right) \quad (1)$$

where  $A_{ij}$  is the correlation function between the spatial points  $i$  and  $j$ ;  $\sigma$  is the standard deviation of the logarithm of liquid limit field;  $\delta$  is the correlation distance and  $d_{ij}$  is the matrix of distances between the center of the elements. Assuming  $d_{ij}^X = d_{ij}^Z$  and  $\delta_X = \delta_Z$  renders the squared exponential form with the advantage of being able to reduce to an isotropic field.

$$A = LL^T \quad (2)$$

where  $A$  is a positive and definitive covariance matrix, the matrix  $L$  can be determined from  $A$  by using the standard

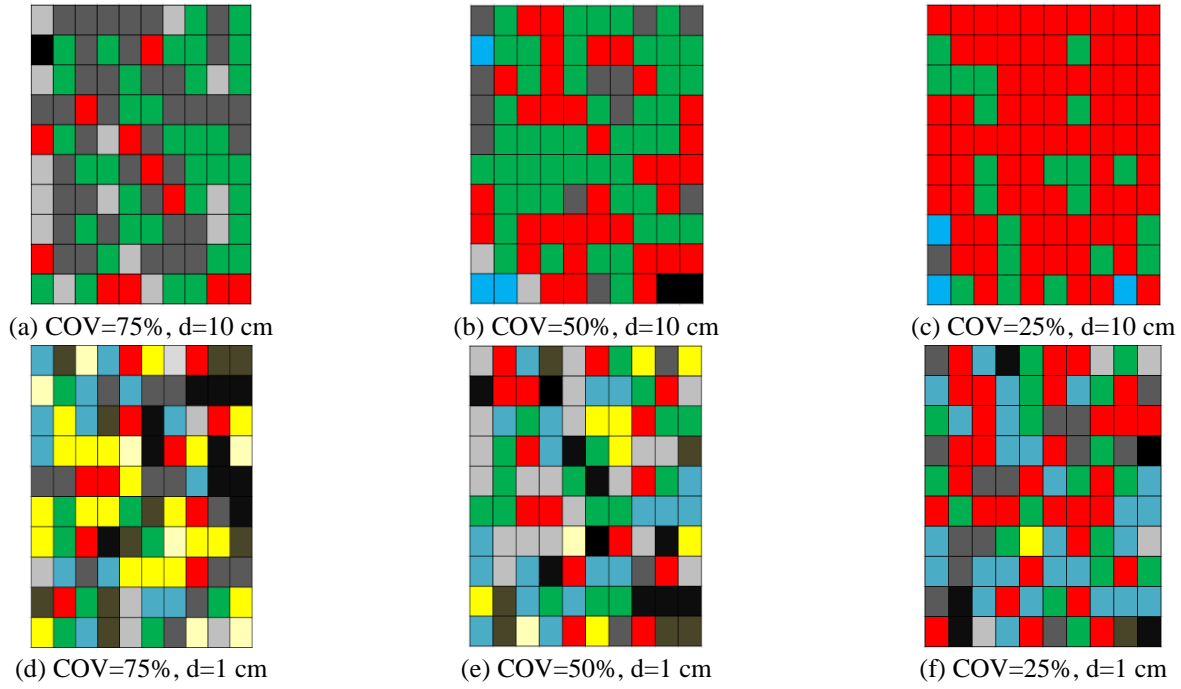


Fig. 2 Isotropic random field generation

Cholesky decomposition technique which decomposes the symmetric and positive definite matrix  $A$ , into a lower triangular matrix. This correlation will then be applied to the random field using Eq. (3).

$$LL = L \cdot \varepsilon + \mu_{\ln LL} \quad (3)$$

where  $L$  is the Cholesky factor of the covariance matrix;  $\varepsilon$  is a vector containing an independent standard normally distributed field  $N(0, 1)$ , and  $\mu$  is a vector containing the mean value of the liquid limit field in logarithmic scale. It was assumed that the liquid limit field bears a lognormal distribution function because it is strictly non-negative. Fig. 1 is a flowchart that shows how the calculations proceed in generating a liquid limit random field. Note that the correlated field (Eq. (3)) will finally convert to log-normal distribution.

Different experiments were used to maintain a constant mean liquid limit, so the coefficient of variation COV and the correlation distance  $\delta$  of the liquid limit stochastic field are the only stochastic parameters investigated in the experimental program. Fig. 2 shows sample realizations of the liquid limit random field. The model is 100 mm  $\times$  100 mm and is divided into 100 square elements that are stochastically isotropic. Fig. 2 shows that the less the correlation distance, the more scattered the random field. Moreover, the higher the variability of the liquid limit stochastic field the wider the spectrum of colors and liquid limit field.

### 3. Experimental test

Physical models were constructed by preparing nine clusters of homogeneous soil with water contents equal to their liquid limits, testing their characteristics to understand

Table 1 Laboratory test schemes

Designatio n	Homogeneous clusters						Heterogeneous reconstituted samples	
	GSA	AL	SP	SG	CT	UCT	Designatio n	DST
S1	☐	☐	☐	☐	☐	☐	DS-1	☐
S2	☐	☐	☐	☐	☐	☐	DS-2	☐
S3	☐	☐	☐	☐	☐	☐	DS-3	☐
S4	☐	☐	☐	☐	☐	☐	DS-4	☐
S5	☐	☐	☐	☐	☐	☐	DS-5	☐
S6	☐	☐	☐	☐	☐	☐	DS-6	☐
S7	☐	☐	☐	☐	☐	☐	-	-
S8	☐	☐	☐	☐	☐	☐	-	-
S9	☐	☐	☐	☐	☐	☐	-	-

Note: ■ = tested; ☐ = not-tested; GSA = Grain Size Analysis; AL = Atterberg Limits; SP = Standard Proctor; SG = Specific Gravity; CT = Consolidation Test; UCT = Unconfined Compression Test; DST = Direct Shear Test

how individual clusters affect the mixtures. Six heterogeneous samples were then constructed and subjected to direct shear tests to investigate their load-displacement behavior in undrained conditions. Table 1 is a summary of the laboratory tests carried out in this study.

#### 3.1 Materials

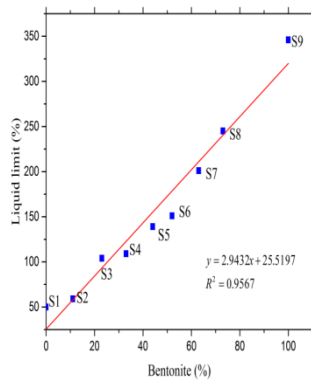
The soils in this study are a combination of commercially available bentonite, kaolin, and colorants; the bentonite and kaolin were sourced locally. Particle size analyses were carried out to establish the percentage of

Table 2 Index properties of the homogeneous clusters

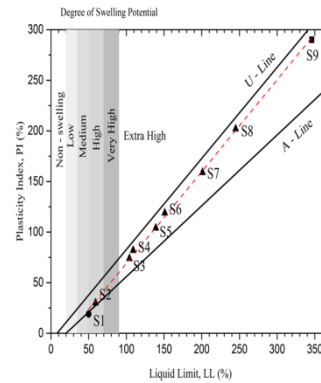
Soil	Atterberg limits									
	K (%)	B (%)	Col (%)	W <sub>L</sub> (%)	W <sub>P</sub> (%)	PI	G <sub>s</sub>	SC	CC (%)	A=PI/clay (< 2μ)
S1	100	0	0	50	31	19	2.59	MH	56	0.34
S2	80	11	9 <sup>a</sup>	59	29	30	2.69	CH	54	0.56
S3	68	23	9 <sup>b</sup>	104	30	74	2.64	CH	57	1.30
S4	55	33	12 <sup>c</sup>	109	27	82	2.61	CH	58	1.41
S5	44	44	12 <sup>d</sup>	139	35	104	2.65	CH	62	1.68
S6	31	52	17 <sup>e</sup>	151	32	119	2.72	CH	61	1.95
S7	20	63	17 <sup>f</sup>	201	42	159	2.75	CH	64	2.48
S8	10	73	17 <sup>g</sup>	245	43	202	2.78	CH	67	3.01
S9	0	100	0	346	56	290	2.80	CH	84	3.45

Note: K = Kaolin; B = Bentonite; Col = Colorant; SC = Soil Classification; CC = Clay Content; A = Activity

<sup>a</sup>Yellow; <sup>b</sup>Combination of 2 % red and 7 % blue; <sup>c</sup>Combination of 4 % red and 8 % blue; <sup>d</sup>Green; <sup>e</sup>Red; <sup>f</sup>Blue; <sup>g</sup>Black



(a) Relationship between the amount of bentonite and the liquid limit



(b) Plasticity chart

Fig. 3 Consistency limits for clusters of homogeneous soil

different grain sizes of kaolin and bentonite. These bentonite and kaolin specimens consist mainly of clay and silt.

Laboratory experiments were carried out to investigate the load-displacement behavior of various soil mixtures that represent the heterogeneous models presented in Table 1.

A consistency limit test, particle size analysis (sieve analysis and hydrometry), specific gravity, compaction, consolidation and unconfined compression tests were carried out according to the ASTM D 4318, ASTM D 422, ASTM D 854 and ASTM D 698, ASTM D 2435 and ASTM D 2166 standards, respectively. Direct shear tests were carried out in accordance with the method proposed by Bro *et al.* (2013) to evaluate the load-displacement behavior of samples of reconstituted heterogeneous soil.

### 3.2 Clusters of homogeneous soil

Nine mixtures were made with different percentages of kaolin, bentonite, and colorant, to differentiate between the nine mixtures. The index properties of the mixtures were characterized in the laboratory and are shown in Table 2.

Liquid and plastic limits are good indicators of the degree of expansion and strength of soils (Grim 1962). The clay content linearly influences the *LL*, *PL*, and *PI* and the

relationship is linear. Increasing the amount of clay will result in higher plasticity and a greater potential for swelling and shrinkage. Fig. 3 shows the relationship between the amount of bentonite and the plasticity parameters.

Casagrande (1948), and later Dumbleton (1968) suggested there are six zones for categorizing the swelling potential of soils; it is presented as a chart with a liquid limit on the abscissa and the plasticity index on the ordinate. The liquid limits and plasticity index of the soil mixtures are plotted on the plasticity chart, as shown in Fig. 3b. The A-line separates the clay and silt such that the clays lie above the line and silt below. All the mixtures fall almost above the A-line, so the soil mixtures are classified as clay. Dakhanamurthy and Raman (1973) stated that the threshold liquid limit that corresponds to high swelling behavior is 50%, as shown in Fig. 3(b).

Bentonite has a higher plasticity and a higher swelling potential than kaolin which has low plasticity and medium swelling potential, but as the percentage of bentonite increases the mixtures approach the U-line. The mixtures S1 and S2 have high swelling potential while other mixtures have a very high potential for swelling. The kaolin-bentonite mixtures are considered as a fine-grained soil with high soil plasticity in soil classification terminology.

Table 3 Compressibility parameters of the samples of reconstituted homogeneous soil

Soil	$e_0^a$	$C_c^b$	$C_s^c$	$C_v(\text{cm}^2/\text{s})^d$
S1	1.07277	0.11860	0.01960	0.61955
S2	1.21720	0.23080	0.03820	0.02109
S3	2.49220	0.39450	0.04120	0.00251
S4	2.10874	0.60370	0.04910	0.00143
S5	2.17488	0.67700	0.04320	0.00104
S6	3.36213	1.27420	0.04630	0.00119
S7	5.13793	1.34740	0.06370	0.00116
S8	3.90134	1.17520	0.10210	0.00072
S9	6.11932	1.35910	0.07230	0.00083

Note: <sup>a</sup>Initial void ratio; <sup>b</sup>Compression index; <sup>c</sup>Recompression index; <sup>d</sup>Coefficient of consolidation at pressure 100 kPa

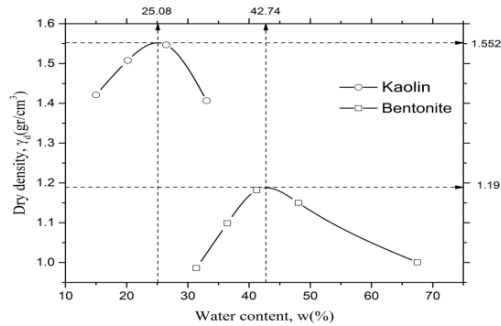


Fig. 4 Proctor standard compaction of kaolin and bentonite

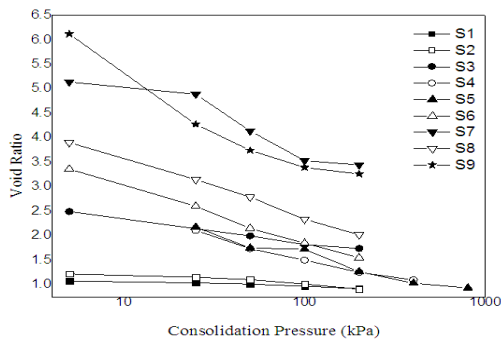


Fig. 5 Variation of void ratio with consolidation pressure for soils

In this study, compaction tests in accordance with ASTM D698 were carried out on kaolin and bentonite to achieve the maximum dry density and optimum water content. Fig. 4 shows that the optimum water content of kaolin and bentonite are lower than their plasticity limit, but the optimum water content of bentonite is higher than kaolin whereas its maximum dry density is lower. The particle size of bentonite is smaller than kaolin and it absorbs more water, and therefore the particles expand and the maximum dry density decreases. Moreover, since the water content at the plastic limit is about 10% more than the optimum water content (Sridharan and Nagaraj, 2005), a value equal to 10% lower than the plasticity limit is assumed as the optimum water content.

Table 4 Results of undrained shear strength from unconfined compression

Soil	$\omega$ (%)	$C_u$ (kPa)	$E$ (MPa)	Soil	$\omega$ (%)	$C_u$ (kPa)	$E$ (MPa)
	31.8	44	3.02		33.3	49	3.70
	32.4	42	2.99		33.8	47.5	3.58
S1	33.1	38	2.81	S6	34.5	46	3.48
	33.9	36	2.53		34.9	44	3.33
	34.6	33	2.35		35.1	42.5	3.21
	30.1	47.5	3.49		38.6	35	3.39
	31.3	44.5	3.26		39.1	34	3.30
S2	31.9	42.5	3.01	S7	39.9	32.5	3.16
	32.5	39	2.82		40.2	31	3.02
	33.9	37.5	2.71		40.8	32	2.95
	30.5	56.5	3.70		40.6	33.5	3.70
	31.5	53.5	3.46		41.3	31.5	3.59
S3	32.2	49	3.24	S8	41.7	30	3.49
	32.9	46	2.91		42.3	29	3.32
	34.1	40	2.72		42.8	27.5	3.22
	28.5	62.5	3.99		43.9	30	3.64
	29.3	59	3.89		44.1	29	3.58
S4	30.1	55	3.68	S9	44.7	27.5	3.31
	31.9	47.5	3.36		45.3	26	3.22
	32.8	45.5	3.01		45.9	25	3.02
	34.6	44	3.29				
	35.2	41	3.06				
S5	35.9	39	2.97				
	36.1	36.5	2.72				
	36.7	32.5	2.53				

Table 5 Results of regression analysis on the physical properties of clusters of homogeneous soil

	$\zeta$	$\eta$	$R^2$		$\zeta$	$\eta$	$R^2$
$C_u-\omega$ (S <sub>1</sub> )	$8 \times 10^{06}$	-3.50	0.99	$E-\omega$ (S <sub>1</sub> )	146232	-3.11	0.96
$C_u-\omega$ (S <sub>2</sub> )	73843	-2.16	0.96	$E-\omega$ (S <sub>2</sub> )	8728.1	-2.30	0.95
$C_u-\omega$ (S <sub>3</sub> )	$3 \times 10^{06}$	-3.16	0.98	$E-\omega$ (S <sub>3</sub> )	78269	-2.91	0.97
$C_u-\omega$ (S <sub>4</sub> )	164057	-2.35	0.99	$E-\omega$ (S <sub>4</sub> )	2819	-1.95	0.96
$C_u-\omega$ (S <sub>5</sub> )	$2 \times 10^{09}$	-4.99	0.94	$E-\omega$ (S <sub>5</sub> )	$2 \times 10^{07}$	-4.41	0.94
$C_u-\omega$ (S <sub>6</sub> )	336550	-2.52	0.95	$E-\omega$ (S <sub>6</sub> )	23098	-2.49	0.94
$C_u-\omega$ (S <sub>7</sub> )	$1 \times 10^{06}$	-2.84	0.99	$E-\omega$ (S <sub>7</sub> )	40887	-2.57	0.98
$C_u-\omega$ (S <sub>8</sub> )	$2 \times 10^{07}$	-3.55	0.99	$E-\omega$ (S <sub>8</sub> )	56964	-2.60	0.98
$C_u-\omega$ (S <sub>9</sub> )	$1 \times 10^{08}$	-4.01	0.99	$E-\omega$ (S <sub>9</sub> )	$2 \times 10^{07}$	-4.11	0.99

One-dimensional consolidation tests were carried out in accordance with ASTM D 2435; nine mixtures were remoulded with their water contents equal to the liquid limit. There are five steps for loading with  $\frac{\Delta p}{p} = 1$  and two steps for unloading; each step lasts for 48 hours. To stop the samples swelling, a pressure of 7 kPa was applied to each mixture before commencing the test. Taylor's method was used to obtain the coefficient of consolidation. The clusters

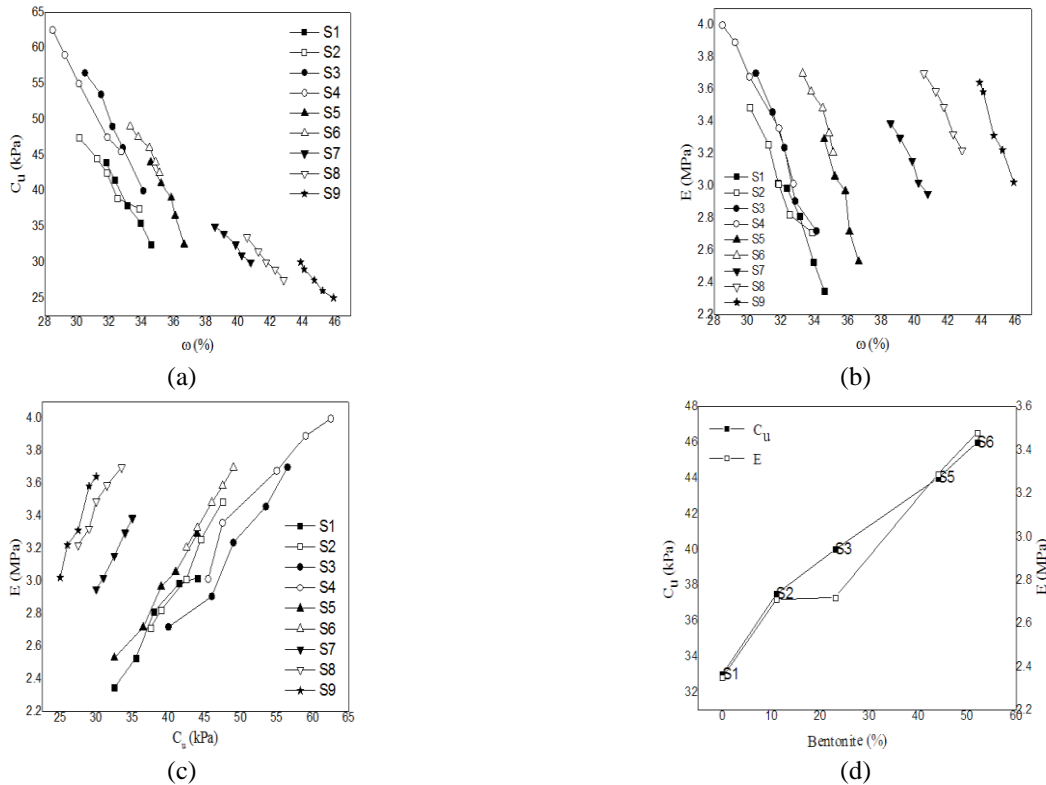


Fig. 6 The results of unconfined compressive strength and stiffness correlations

of homogeneous soil underwent consolidation tests to evaluate their individual compressibility and then use the results for predicting their load-displacement behavior in direct shear tests. Fig. 5 shows the variation of the void ratio with consolidation pressure. Increasing the amount of bentonite generally leads to higher void ratios, but there are two exceptions: for the S3 and S7 soils the void ratios lie above those soils with higher amounts of bentonite. The compressibility parameters acquired from consolidating different clusters are shown in Table 3. Here the initial void ratio obtained before consolidation, and the compression index and recompression index increased as the amount of bentonite increased.

### 3.3 Unconfined compression tests

These tests are to measure the uniaxial compressive strength of cohesive soil under a uniaxial load or strain-controlled conditions, according to ASTM-D2166. Five experiments were carried out on each sample where the water content was higher than the corresponding plasticity limit, and then their unconfined compressive strength was determined. The results of the unconfined compression tests (UCT) are shown in Table 4. The cohesions of soil, particularly fine-grained soils, depends largely on the molecular link that each grain has with the absorbed water; this is why the value of cohesion changes with the soil water content and the amount of different minerals. For example, by increasing the water content the cohesion of clay will decrease due to the larger separation between grains. The soil water content is the most important factor in the compaction of clay soils. Soil compacted at a water content that is higher than the optimum water content,

behave contrary to soils which are dry of optimum.

A relationship can be developed for each test between the water content and undrained shear strength and also the unconfined deformation modulus by using regression analysis and adopting the model proposed by Koumoto and Houlsby (2001) and Trauner *et al.* (2005) with the general form of  $C_u$  (or  $E$ ) =  $\zeta \omega^{-n}$ . Fig. 6 shows UCT curves of the nine clusters. It is apparent that both the undrained cohesion and the unconfined compression modulus decrease with increasing water content. Another observation is that the unconfined compression modulus is lineally proportional to the undrained cohesion as appears from Fig. 6(c). Furthermore, it is observed that the compacted bentonite soil has the highest compressive strength and a higher deformation modulus. The unconfined compressive strength and stiffness increased almost lineally as the amount of bentonite in kaolin-bentonite mixtures increased (Fig. 6(d)).

Table 5 presents the regression analyses for the variation of undrained shear strength and elastic deformation modulus with water content from the UCT tests.

### 3.4 Reconstitution of heterogeneous soil

Once the nine clusters were prepared with water contents equal to their corresponding liquid limit, they were injected and pasted into a perforated box to match the numerically realized pattern based on random field theory. The wooden box was 150 mm deep, 100 mm wide and 100 mm long. The side walls and bottom plates were perforated to allow for drainage. All the walls and the bottom of the box were covered with filter sheets to prevent the drainage holes from being blocked (Fig. 7(a)). Six heterogeneous

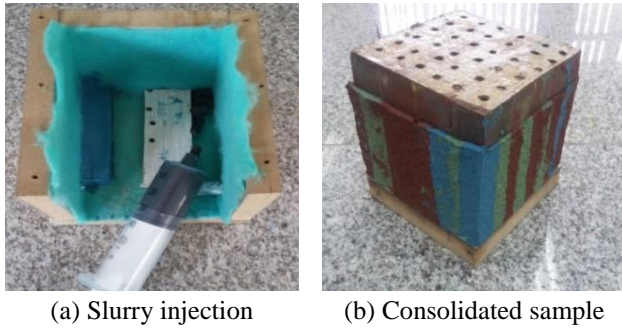


Fig. 7 Consolidation process

Table 6 Summary of the shear testing program on samples of reconstituted heterogeneous soil

Designation	Stochastic Parameters		$\sigma_n$ (kPa)
	COV <sup>a</sup> (%)	$\delta^b$ (cm)	
DS-1	25	1	100, 200, 300
DS-2	50	1	100, 200, 300
DS-3	75	1	100, 200, 300
DS-4 Table 6 Summary of the shear testing program on samples of reconstituted heterogeneous soil	25	10	100, 200, 300
DS-5	50	10	100, 200, 300
DS-6	75	10	100, 200, 300

Note: a=Coefficient of variation and b=Autocorrelation distance

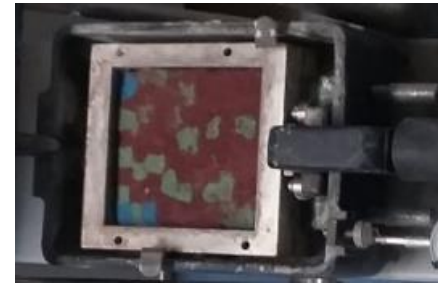
models with different stochastic parameters were constructed by placing strings of slurry into a box with a syringe. A hundred elements of the random field were placed one by one in layers starting from the bottom of the box (Fig. 7(a)). Once the heterogeneous sample had been constructed it was subjected to consolidation.

### 3.5 Consolidation process

The first stage of consolidation was one-dimensional compression in a constrained condition. The box was tied up with metal wire to constrain the model laterally. Vertical stresses of 25 kPa, 50 kPa, and 100 kPa were applied to the soil. Each stress remained on the soil for 48 hours to accomplish primary consolidation, during which the water drained out vertically and horizontally. After consolidation the perforated box was opened and the filter pads were removed (Fig. 7(b)). The height of the soil after consolidation was about 90 mm, and it was divided into three parts with a cutter for the next stage. To reach 200 kPa of consolidation, each sample was transported to the direct shear box so that the overburden pressure could be applied.

### 3.6 Direct shear tests

There are many ways to measure and address the shear strength of soil as described in most geotechnical engineering textbooks. In most cases, a Mohr failure envelope is used where the shear strength (usually peak, critical state, or residual) is plotted as a function of the



(a) Shearing process



(b) Sheared heterogeneous model

Fig. 8 Direct shear test

Table 7 Direct shear test and undrained cohesion calculations

Designation	Model Dimension (cm)	$(C_u)_{DS}$ (kPa)	$(C_u)_{mean}$ (kPa)
DS-1	$10 \times 10 \times (1.6, 1.5, 2)$	19.29	18.8
DS-2	$10 \times 10 \times (1.5, 1.7, 1.8)$	18.72	18.4
DS-3	$10 \times 10 \times (2, 2, 2)$	20.93	19.4
DS-4	$10 \times 10 \times (2.7, 3, 2.8)$	26.08	25.3
DS-5	$10 \times 10 \times (3, 3, 2.7)$	25.16	22.0
DS-6	$10 \times 10 \times (2, 2, 2.7)$	22.40	19.7

Note:  $(C_u)_{DS}$  = Undrained cohesion from direct shear test,  $(C_u)_{mean}$  = Mean undrained cohesion from water content correlations

direct effective stress on the failure plane, or a modified Mohr diagram is used where the maximum shear stress versus the average of the major and minor principal effective stresses at failure is plotted. A number of studies (Hvorslev 1961, Gibson 1953, Schmertmann and Osterberg 1960 and Schmertmann 1964), indicated that the total strength of a clay consists of two distinct parts: a cohesion that depends only on the void ratio (water content), and a frictional contribution that only depends on the normal effective stress. These two parts are evaluated by measuring the strength of the two samples at the same void ratio or water content, but at different levels of effective stress.

This study evaluates the undrained shear strength through direct shear tests and the correlation from unconfined compression tests. Consolidated undrained tests proposed by Bro *et al.* (2013) were carried out. A standard guideline such as ASTM D 3080 is suitable for consolidated drained conditions. Undrained conditions are widely used and applicable in many geotechnical problems such as when dynamic loads affect the soil and there is not enough time for drainage. The undrained shear strength of fine-grained

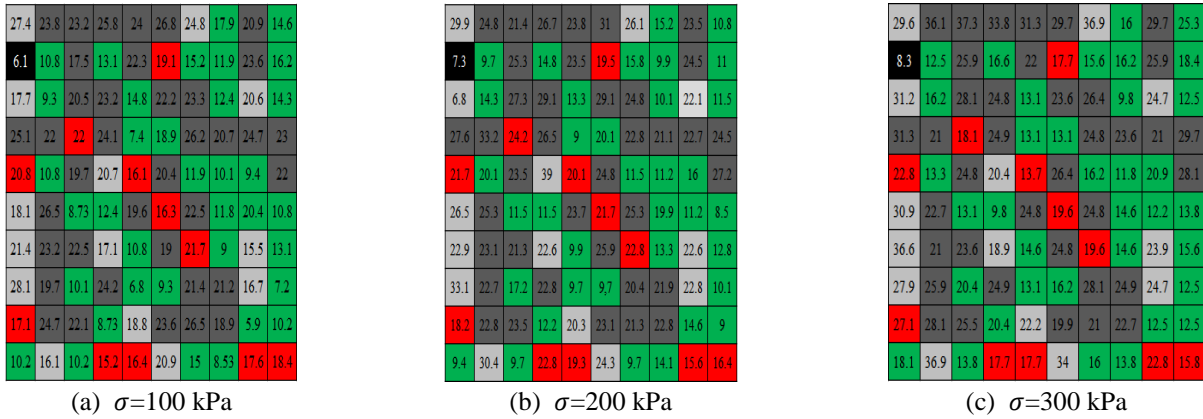


Fig. 9 2D realizations of undrained cohesion, COV=75%,  $\delta=10$  cm

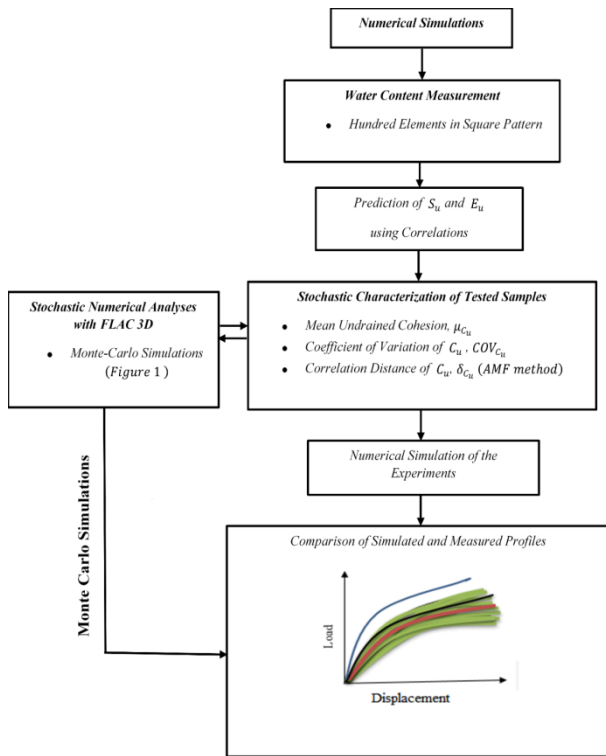


Fig. 10 Flowchart for Monte Carlo simulations

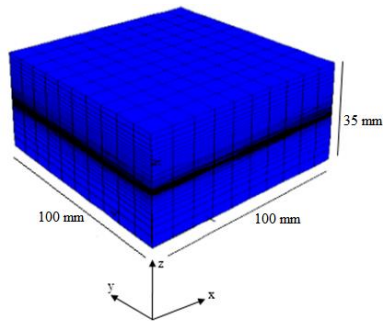


Fig. 11 The model geometry and 3D mesh in the direct shear test simulations

soils in this situation is called undrained cohesion  $C_u$ , and it depends on the initial porosity or the water content of the soil. In this study the average time for reaching 50% consolidation was calculated based on the

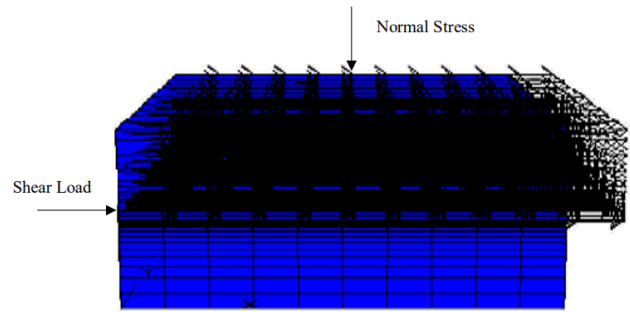


Fig. 12 Apply velocity and stress field to the upper box

consolidation results for homogeneous mixtures, shown as  $t_{50}$ . In an undrained direct shear test, shearing should happen fast enough to avoid a change of volume due to drainage so the time for failure  $t_f$  used in this study was equal to  $0.1t_{50avg}$  where  $t_{50avg}$  is the average time needed for nine mixtures to reach 50% consolidation.

Once the six heterogeneous samples had consolidated, direct shear tests were carried out according to the method proposed by Bro *et al.* (2013). Table 6 presents the direct shear test program for the six heterogeneous models. The soil had a wet density of approximately  $1.68 \text{ gr/cm}^3$  and water content after the test which varied from 40% to 50%. Fig. 8 shows a heterogeneous sample placed in the direct shear box. A consolidated undrained direct shear test was utilized in accordance with the unconfined compression test and the applied strain rate should be fast enough to avoid drainage, so it was fixed at 1 mm per minute. Normal stresses applied to each heterogeneous sample were 100 kPa, 200 kPa, and 300 kPa. Fig. 8(b) shows the sheared sample after the direct shear test had been completed.

The direct shear box is  $100 \text{ mm} \times 100 \text{ mm} \times 4 \text{ cm}$  and it was used to fulfill the experimental aspect of this study. As mentioned earlier, heterogeneous samples were made in the laboratory to the same dimensions but with a height of 15 cm. Because each sample should have been tested under three normal stresses, they were cut twice and then placed in the direct shear box; this is why the heights of the samples introduced in Table 7 are not the same. Undrained cohesion was back calculated in two different ways. The results of direct shear tests with different overburden pressures were used collectively in order to estimate the cohesion values. In the element scale the correlations

Table 8 Stochastic parameters measured from the experimental simulations

Designation	$\mu_{C_u}$ (kPa)	$COV_{C_u}$ (%)	$\delta_{C_u}$ (cm)
DS-1	18.8	39	1
DS-2	18.4	34	1
DS-3	19.4	48	1
DS-4	25.3	29	10
DS-5	22.0	38	10
DS-6	19.7	34	10

between the water content and undrained cohesion were used to estimate the field of cohesion within the specimens, while the mean value was compared with the integral view values. Table 7 shows the computed undrained cohesion values for different experimental models that will be used in a numerical analysis scheme for further stochastic simulations and analyses.

### 3.7 Numerical simulations

Over the past few decades, researchers have used different software to model the direct shear test procedure; for instance, Bagherzadeh Khalkhali and Mirghasemi (2009) used the software ELLIPSE to model direct shear tests, while Park and Song (2009) used *PFC<sup>3D</sup>* software to simulate direct shear tests. Numerical modelling in this study is separated into a simulation of the experimental test set-up and parametric studies; *FLAC<sup>3D</sup>* was used for this purpose.

*FLAC<sup>3D</sup>* is a three-dimensional finite difference program that is usually used to simulate rock-structure or soil-structure interactions which undergoes plastic deformation when they reach their respective yield limits. *FLAC<sup>3D</sup>* is better at simulating the exact test procedures and finite boundary conditions used in physical laboratory direct shear tests.

Heterogeneous samples were made from a realization of the nine soil samples with different mechanical properties; these mechanical properties were estimated using a sampling applicator to capture the water content of the hundred constituting elements. Samples were taken as fast as possible to avoid any loss or redistribution of water, and then cohesion was calculated through the relationships obtained previously in Table 5. Fig. 9 shows the values of the undrained shear strength inferred from the correlated water contents with increasing overburden pressure, as shown in Fig. 9, where the element scale of the sample water content has been reduced and undrained cohesion has then increased.

The mapped shear strength and deformation parameters were incorporated into the numerical analysis scheme in order to complete the numerical simulation. Obviously, the next step will be to compare the predicted load-displacement with the experimental results.

Numerical analyses carried out in this current research can be divided into two categories where the first series is related to the back analyses of direct shear tests carried out on random heterogeneous reconstituted samples. The Monte

Carlo simulation technique was then used to produce various possible realizations of heterogeneous samples with the same stochastic properties. Fig. 10 is a flowchart that shows how the stochastic and deterministic numerical analyses of the first category proceeded. The Monte Carlo reproduction of experimental load-displacement results were carried out by calculating the mean undrained cohesion,  $\mu_{C_u}$ , the coefficient of variation of  $C_u$ , and the  $COV_{C_u}$  and correlation distance of  $C_u$ ,  $\delta_{C_u}$  from the experiments (Table 8).

#### 3.7.1 Model geometry

A series of 3D finite difference analyses were carried out to simulate direct shear tests using *FLAC<sup>3D</sup>*. The model geometry is shown in Fig. 11. The metal box of the direct shear apparatus was modelled with rigid surfaces in the numerical model.

Three material zones were needed in the modelling direct shear tests; namely the soil specimen in two halves, as well as the top and a solid cap for the shear box. The soil material and the top cap were modelled using rectangular *FLAC* elements (i.e., four points and four sides). The dimension in the  $z$ -direction of each sample is different (Table 7), but it is similar to the laboratory soil specimen in the direct shear box. The model mesh is shown in Fig. 11 (the elements at each level are 10 mm  $\times$  10 mm).

#### 3.7.2 Loading condition and choice of constitutive model

The analysis was carried out in two steps; in the first step only, normal stress was applied on the top surface of the model and in the second step, shear stress was applied in a stepwise scheme. All the analyses were carried out using normal stresses of 100 kPa, 200 kPa, and 300 kPa. The normal stress values were the same as those used in the experimental program. Each model in *FLAC<sup>3D</sup>* was developed to represent a specific type of constitutive behavior commonly associated with the geologic material. The Mohr-Coulomb plasticity model was used for materials that yield when subjected to shear loading, but the yield stress only depends on the major and minor principal stresses' the intermediate principal stress has no effect on yielding. A Mohr-Coulomb material model was initially defined for all zones. In Monte Carlo simulations, the soil parameters are distributed randomly between elements in each realization, but as the number of realisations increase the shear strength approaches an almost constant value. There were 500 realizations in each set of analyses.

#### 3.7.3 Boundary conditions

The lowermost boundary of the model is fixed in the  $x$ ,  $y$  and  $z$  directions, but in the first step both sides were fixed in the  $x$  and  $y$ -direction to allow the specimen to consolidate vertically, but not laterally; this is consistent with the mechanism of the physical shear box test. In the second step, the lateral walls of the bottom box are fixed in the  $x$  and  $y$  directions (horizontal plane) and a horizontal velocity of about  $(6.67 \times 10^{-4} \text{ cm/s})$  was applied to the upper box in the  $x$  direction (Fig. 12).

## 4. Results of experimental and numerical simulation

Six heterogeneous models formed through random field

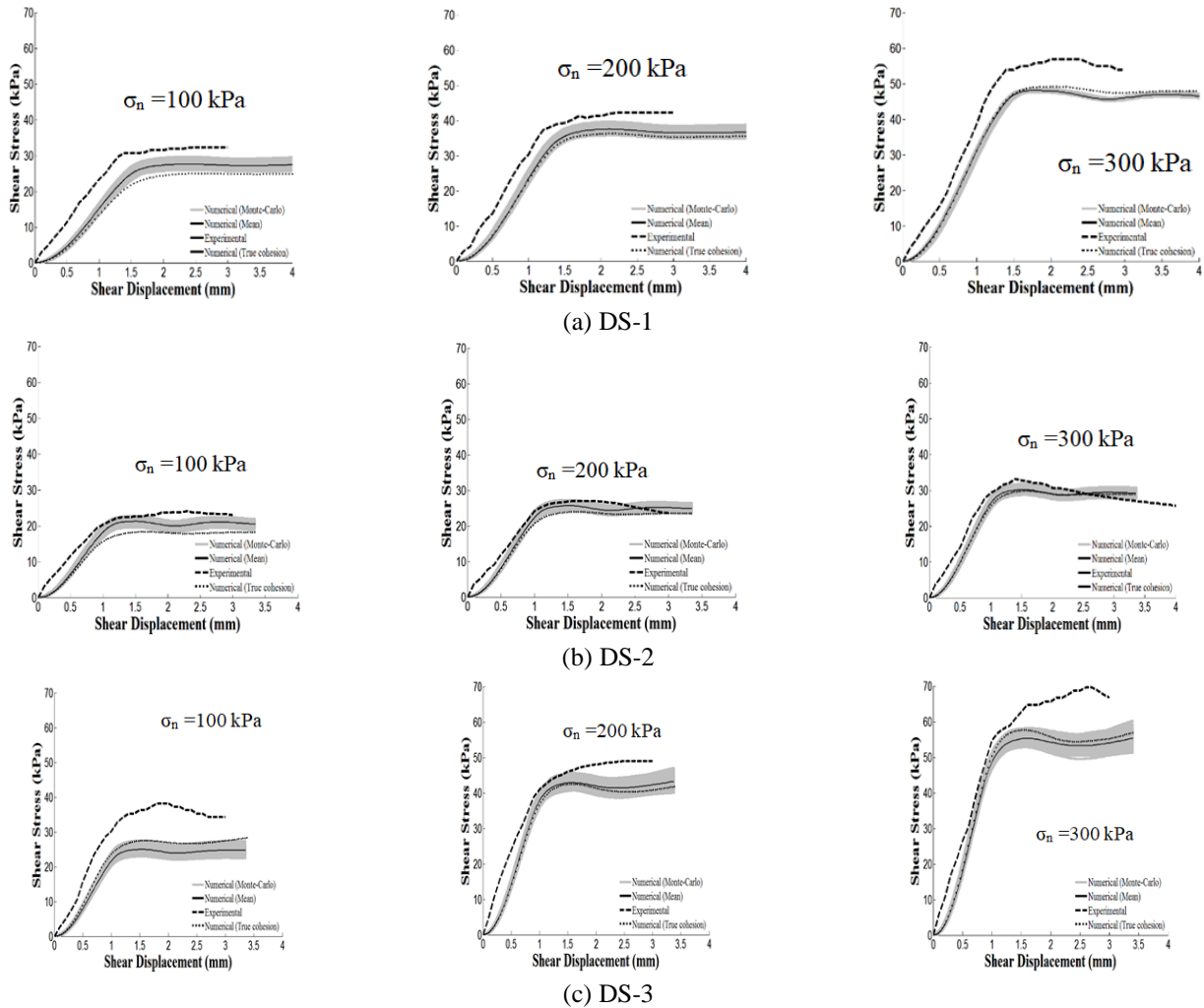


Fig. 13 Comparison of experimental and numerical modelling of direct shear tests on heterogeneous reconstituted soil samples

theory calculations were tested in a direct shear test machine. 100 elements were set in square pattern to reflect their specific stochastic properties. Although randomness cannot be fully simulated by constructing a limited number of heterogeneous models, each model represents one realisation out of many different possible randomised patterns bearing the same stochastic properties. After each test, one hundred samples were taken to map the water content in each model. Correlations were produced to determine the shear strength and stiffness in different elements. The shear strength and stiffness fields were then implemented into the  $FLAC^{3D}$  numerical analysis package to simulate the load-displacement profiles of direct shear condition. This section will discuss how well the experimental and numerical load-displacement profiles compare with each other.

Figs. 13 and 14 show the shear stress-shear displacement profiles for different heterogeneous models with three overburden pressures. Different types of load-displacement profiles were delineated for each model for comparison. The experimental direct shear load-displacement curves are plotted along with the results of the numerical simulation. Two numerical analyses were carried

out; the first was a direct simulation of the physical realisation used to prepare the sample for experiments and the second category was in the form of Monte Carlo simulations where stochastic properties were inherited from each real and physical realisation after the test finished. A spectrum of load-displacement profiles superimposed with their mean profile are shown on all the graphs, and observations are drawn when comparing the different profiles.

As expected, in most cases the numerical analysis corresponding to the physical realisation fell within the Monte Carlo simulations spectrum which means that each physical simulation of randomness and heterogeneity was only one possible realisation among all and therefore it is not deterministic; in fact it belongs to a stochastic family with specified properties. Another interesting observation was that in all cases the load-displacement curves corresponding to laboratory experiments were above the possible spectra, as predicted by numerical analyses. This consistent behaviour can only occur because the constitutive parameters adopted in the numerical analysis section are based on the findings of unconfined compression tests. However, the lateral deformation

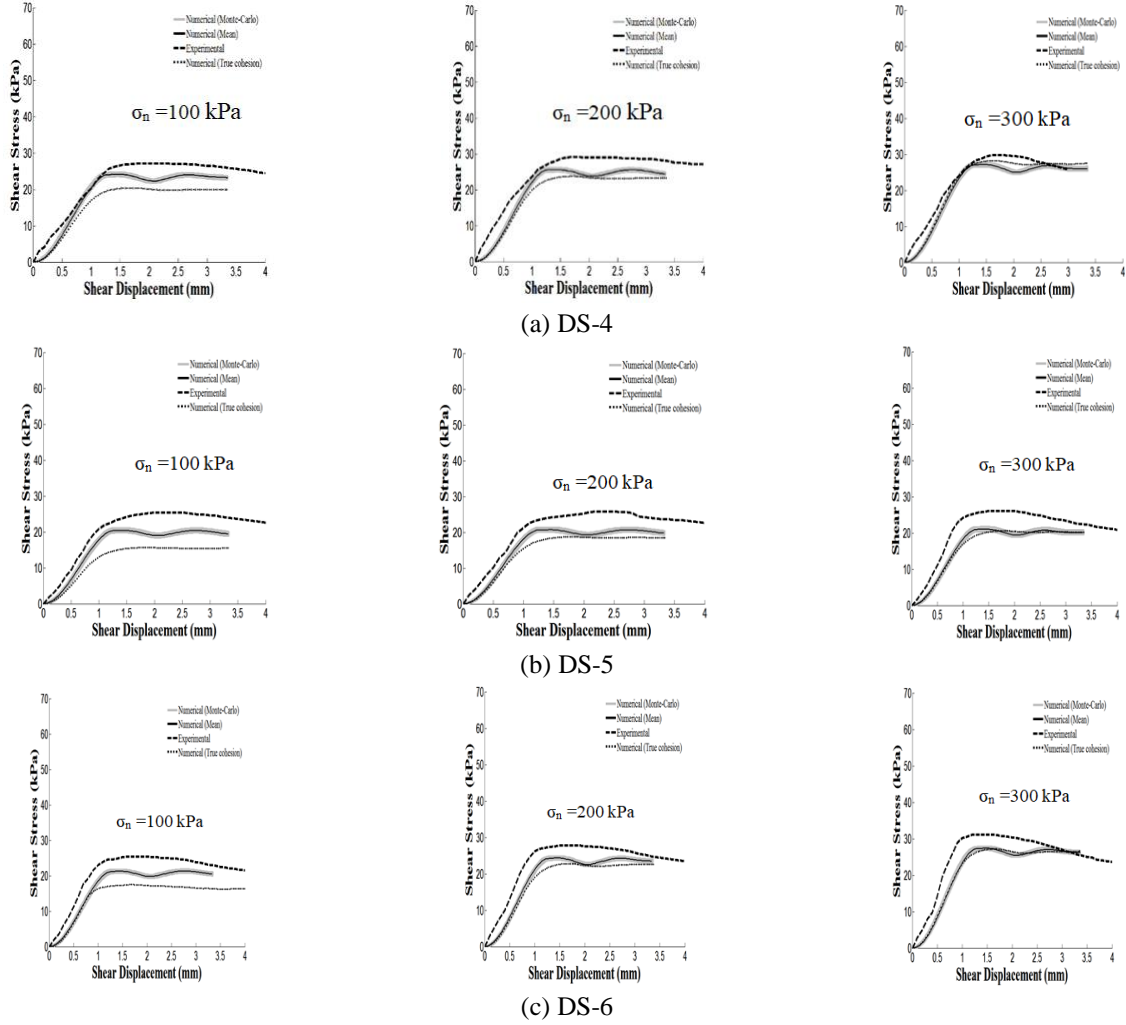


Fig. 14 Comparison of experimental and numerical modelling of direct shear tests on heterogeneous reconstituted soil samples

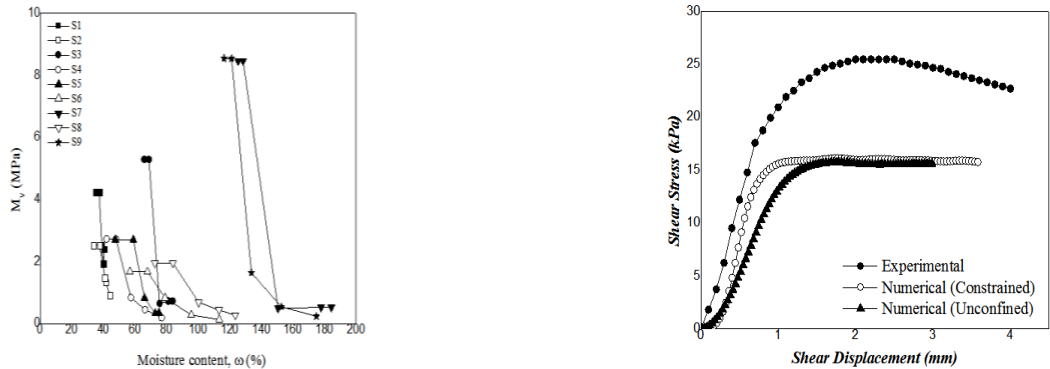


Fig. 15 Effect of constrained lateral deformation condition on load-deformation prediction accuracy

conditions in the direct shear machine was constrained and no horizontal deformation in the upper and lower halves were allowed. This means that using the results of unconfined compression tests in strength and stiffness correlations should lead to lower bound load-displacement curves. Eq. (4) illustrates how the constraint deformation modulus can be converted from a triaxial compression

modulus if Poisson's ratio is available.

$$E_{Oed} = \frac{(1 - \nu)}{(1 + \nu)(1 - 2\nu)} E_{TC} \quad (4)$$

where  $E_{Oed}$  is the Oedometric (constraint) compression modulus obtained from an Oedometric test,  $\nu$  is the Poisson's ratio and  $E_{TC}$  is the triaxial compression modulus



(a) Slurry injection (b) Longitudinal joints

Fig. 16 Substantiation of uneven or irregular surfaces during elemental injections

measured from a conventional triaxial test.

Oedometric (Constraint) deformation modulus as introduced in Eq. (4) can be directly measured from the oedometric experiments as illustrated in Fig. 6. The Oedometric deformation modulus is a function of the void ratio which is interchangeable with the moisture content. This means that the oedometric deformation modulus can be correlated with the moisture content for samples with different bentonite contents. If the unconfined compression moduli adopted in numerical simulations are superseded by the new correlated constraint moduli as illustrated in Fig. 15, the results of the numerical simulations of the load-deformation profiles will change and more conformity will be reached. This conformity as noted, is only for deformation behavior, however, the simulated ultimate shear stress of the heterogeneous sample still deviates substantially from the experimental result. This is again because the shear strength parameters, the undrained shear strength in this case, is correlated from unconfined compression tests as pointed out earlier. This deviation is also expected to get resolved if direct shear test results, similar to current heterogeneous test conditions, are employed for finding the shear strength-moisture content correlations.

Another source of disagreement emanates from the sample preparation method which presumably leaves rough and ragged interfaces between elements longitudinally (Fig. 16); this condition escalates when plasticity gradients are expected between adjacent and randomly defined elements and become more prominent when a high coefficient of variation or a low scale of fluctuations are adopted. Fig. 13 (c) corresponds to the highest variability and lowest correlation and thus shows a more highlighted discrepancy between the experimental and numerical results. Lastly, but not as important, is the fact that the strength and stiffness correlations in unconfined condition lack information on the loading, unloading, and reloading that occurred when preparing the direct shear samples. This may cause the correlated strength and stiffness to deviate from the true values obtained after each direct shear experiment. These three possible sources of deviation will collectively cause the predicted load-displacement profiles to depart from the experimental curves.

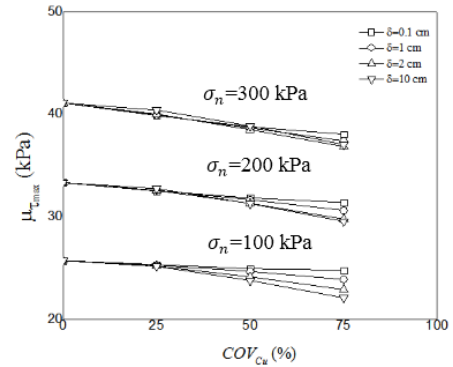


Fig. 17 Effect of the variability of the undrained cohesion on the mean shear strength,  $\mu_{C_u}=20$  kPa

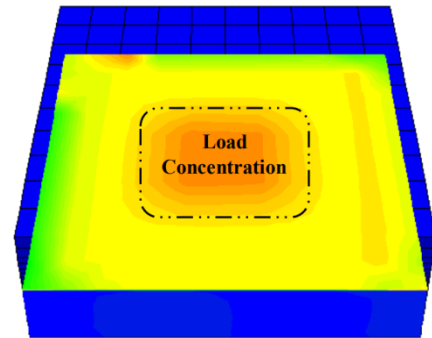


Fig. 18 Shear stress concentration in direct shear sample,  $\mu_{C_u}=20$  kPa

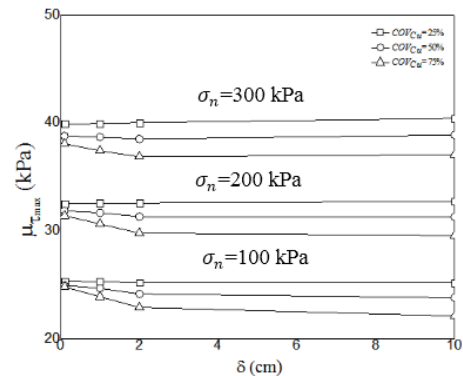


Fig. 19 Effect of correlation distance of undrained cohesion on the mean shear strength,  $\mu_{C_u}=20$  kPa

## 5. Results of Parametric study

The main objective of the parametric study was to determine how the coefficient of variation and correlation distance of the undrained cohesion affected the shear strength obtained from direct shear tests. Cherubini *et al.* (1993) and Phoon and Kulhawy (1999) concluded that the coefficient of variation had an inverse effect on the undrained shear strength. Fig. 17 shows the variation of the mean shear strength in direct shear condition with the coefficient of variation of undrained cohesion.

Fig. 17 shows that the maximum shear stress in direct shear has decreased in average sense as the variability of the undrained cohesion ( $COV_{C_u}$ ) increased. The compulsory shearing mechanism in the direct shear machine enables the

shear strength field to affect the failure strength in an average sense, albeit a variable cohesion field with a constant mean value does not necessarily render the same overall shear strength, but even though the mean is constant, the shear stress concentrates in the center of the plane, as shown in Fig. 18. This means that the contribution made by the central and marginal zones to mobilize the interface shear stress should be different; but if a uniform cohesion field is adopted the final shear stress corresponding to failure will presumably reach the yield condition by the readjustment and redistribution of the stress states in different zones. However, when a heterogeneous cohesion field is realized, the ultimate shear strength in each realization will depend on whether the central zones are assigned as “strong” or “weak” states. This implies that the ultimate shear strength of heterogeneous models will depend on whether the central zones are occupied by the so-called “strong” state. Random field theory will produce lots of realizations through the Monte Carlo simulation technic, but only some will constitute a strong state in the central zones. This will create reduced mean shear strength due to the adoption of a random variable cohesion field, and therefore the mean shear strength is expected to decrease as the variability increases, as shown in Fig. 17.

Further observation was made by analyzing the graphs delineated in Fig. 17; here the effect that the correlation distance has on the mean direct shear strength is marginal. Fig. 19 shows a clear picture of the variation regime of the mean direct shear strength with the correlation distance of the random cohesion field. It is deduced that the mean direct shear strength decreased slightly with the correlation distance, but this reduction stops for longer correlations because a forced and compulsory failure surface in the direct shear experiments entitled the shear strength to vary with the degree of closeness of more cohesive zones to the central loading area where stress concentration happens. The failure surface has divided into two distinct zones: the central concentration zone and the rim (Fig. 18). In each zone the shear strength has accumulated as the shear stresses accumulated in different elements of each zone, and therefore the correlation distance will not affect the overall shear strength.

## 6. Conclusions

In geotechnical engineering analysis, many of the mechanical properties of earthen materials are inherently variable and heterogeneous, and therefore uncertainty is an important property in geotechnical engineering practices. The uncertainty of soil properties has been widely studied using a variety of numerical models and random field theory. This paper presents a new outlook to model inherent variability in the laboratory by preparing reduced-scale direct shear models. To achieve this, six physical realizations from simulated random field models were reproduced and substantiated physically by varying the mineralogy, as manifested by the amount of bentonite and kaolin. The liquid limit, proven to vary linearly with the amount of bentonite, represented a random field, each

element in the discretized model was assigned a prescribed amount of bentonite according to the realized liquid limit. Each cluster was pasted at a water content that corresponded to its liquid limit. The direct shear model was then consolidated in two stages. The heterogeneous samples then underwent direct shear loading to obtain the shear load-displacement profile of each sample. A correlation was made between the water content and strength parameters through an independent unconfined compression test for each homogeneous cluster with different amounts of bentonite and kaolin. These correlations were used to map the real stochastic properties of each tested sample by only measuring the water content at each isolated element of the heterogeneous models. These stochastic properties were then implemented into a random finite difference analysis procedure to simulate the experimental load-displacement profiles.

A comparison of the experimental and numerical Monte Carlo simulations revealed some sources of deviation which should be considered before seeking closely conforming results. The difference between unconfined and confined compression test conditions, a ragged interface between elements and the effect of the loading history on the strength and stiffness correlations are presumed to be the most important.

Sets of parametric studies were undertaken to numerically determine how different stochastic parameters affected the direct shear strength. It was found that only the coefficient of variation of a cohesion field affected the mean direct shear strength, but the correlation distance had almost no effect in a direct shear condition where the concentration of stress in the central elements controlled the situation.

The method proposed in this paper offers a new technique for constructing and studying the issue of soil variability in ordinary shear loading conditions, and the method used to prepare the samples can be generalized and extended to different geotechnical problems. However, to efficiently implement the experimental results into practical numerical analysis the potential sources of deviation arising from the sample preparation routine and the loading history and condition must be interpreted and discussed carefully.

## Acknowledgements

The direct shear tests were conducted utilizing the direct shear test apparatus of the Ferdowsi University and the authors would like to acknowledge with thanks the supports from the staff of the laboratory of soil mechanics.

## References

- Al-Bittar, T. and Soubra, A.H. (2013), “Bearing capacity of strip footings on spatially random soils using sparse polynomial chaos expansion”, *Int. J. Numer. Anal. Meth. Geomech.*, **37**(13), 2039-2060.
- American Society for Testing and Materials, (1999), *Standard Test Method for Laboratory Compaction Characteristics of Soil Using Standard Effort (12400 ft-lb f/ft<sup>3</sup>(600kn-m/m<sup>3</sup>))*, Annual Book of ASTM Standards, ASTM D698, Vol.4.08, ASTM International, West Conshohocken, Pennsylvania, U.S.A.

- ASTM, D. 1994. 4318-93 (1994), *Standard Test Method for the Liquid Limit, Plastic Limit and Plasticity Index of Soils*, in *Annual Book of ASTM Standards*, ASTM International, West Conshohocken, Pennsylvania, U.S.A., 551-561.
- ASTM D 854-02 (2013), *Standard Test Methods for Specific Gravity of Soil Solids by Water Pycnometer*, ASTM International, West Conshohocken, Pennsylvania, U.S.A.
- ASTM D.2166, (2016), *Standard Test Method for Unconfined Compressive Strength of Cohesive Soil*, ASTM International, West Conshohocken, Pennsylvania, U.S.A.
- ASTM D 698-07 (2013), *Standard Test Methods for Laboratory Compaction Characteristics of Soil Using Standard Effort*, ASTM International, West Conshohocken, Pennsylvania, U.S.A.
- ASTM, D. 2435-96. (1998), *Standard Test Method for One-dimensional Consolidation Properties of Soils*, in *Annual Book of ASTM Standards*, ASTM International, West Conshohocken, Pennsylvania, U.S.A.
- Azari, B., Fatahi, B. and Khabbaz, H. (2016), "Assessment of the elastic-viscoplastic behavior of soft soils improved with vertical drains capturing reduced shear strength of a disturbed zone", *Int. J. Geomech.*, **16**(1), B4014001
- Bagherzadeh-Khalkhali, A. and Mirghasemi, A.A. (2009), "Numerical and experimental direct shear tests for coarse-grained soils", *Particuology*, **7**(1), 83-91.
- Bro, A.D., Stewart, J.P. and Pradel, D. (2013), "Estimating undrained strength of clays from direct shear testing at fast displacement rates", *Proceedings of the Geo-Congress 2013: Stability and Performance of Slopes and Embankments III*, San Diego, California, U.S.A.
- Dakshnamurthy, V. and Raman, V. (1973), "A simple method of identifying an expansive soil", *Soil. Found.*, **13**(1), 97-104.
- Deb, K. and Majee, A. (2014), "Probability-based design charts for stone column-improved ground", *Geomech. Eng.*, **7**(5), 539-552.
- El-Emam, M., Attom, M. and Khan, Z. (2012), "Numerical prediction of plane strain properties of sandy soil from direct shear test", *Int. J. Geotech. Eng.*, **6**(1), 79-90.
- El-Kadi, A.I. and Williams, S.A. (2000), "Generating two-dimensional fields of autocorrelated, normally distributed parameters by the matrix decomposition technique", *Groundwater*, **38**(4), 530-532.
- Fenton, G.A. and Griffiths, D.V. (2002), "Probabilistic foundation settlement on spatially random soil", *J. Geotech. Geoenviron. Eng.*, **128**(5), 381-390.
- Fenton, G.A. and Griffiths, D.V. (2003), "Bearing-capacity prediction of spatially random  $c$   $\phi$  soils", *Can. Geotech. J.*, **40**(1), 54-65.
- Fenton, G.A. and Griffiths D.V. (2008), *Risk Assessment in Geotechnical Engineering*, Wiley, New York, U.S.A.
- Garzón, L.X., Caicedo, B., Sánchez-Silva, M. and Phoon, K.K. (2015), "Physical modelling of soil uncertainty", *Int. J. Phys. Modell. Geotech.*, **15**(1), 19-34.
- Gibson, R.E. (1953), "Experimental determination of the true cohesion and true angle of internal friction in clays", *Proceedings of the 3rd International Conference of Soil Mechanics and Foundation Engineering (ICSMFE)*, Switzerland, August.
- Griffiths, D.V., Fenton, G.A. and Manoharan, N. (2006), "Undrained bearing capacity of two-strip footings on spatially random soil", *Int. J. Geomech.*, **6**(6), 421-427.
- Grim, R.E. (1962), "Applied clay mineralogy", *Science*, **135** (3507), 890-898.
- GuhaRay, A. and Baidya, D.K. (2014), "Partial safety factors for retaining walls and slopes: A reliability-based approach", *Geomech. Eng.*, **6**(2), 99-115.
- Halder, S. and Babu, G.S. (2008), "Effect of soil spatial variability on the response of laterally loaded pile in undrained clay", *Comput. Geotech.*, **35**(4), 537-547.
- Hicks, M.A. and Spencer, W.A. (2010), "Influence of heterogeneity on the reliability and failure of a long 3D slope", *Comput. Geotech.*, **37**(7), 948-955.
- Huang, X.C., Zhou, X.P., Ma, W., Niu, Y.W. and Wang, Y.T., (2016), "Two-dimensional stability assessment of rock slopes based on random field", *Int. J. Geomech.*, **17**(7), 04016155.
- Hvorslev, M.J. (1961), *Physical Components of the Shear Strength of Saturated Clays (No. WES-MP-3-428)*, Army Engineer Waterways Experiment Station, Vicksburg, Mississippi, U.S.A.
- Jamshidi Chenari, R. and Oloomi Dodaran, R. (2011), "Evaluation of the heterogeneity in deformability of natural alluvial deposits using random field theory", *Sharif J. Sci. Res.*, **27**(4), 75-83.
- Jamshidi Chenari, R. and Mahigir, A. (2014), "The effect of spatial variability and anisotropy of soils on bearing capacity of shallow foundations", *Civ. Eng. Infrastruct. J.*, **47**(2), 199-213.
- Jamshidi Chenari, R., Zhalehjo, N. and Karimian, A. (2014), "Estimation on bearing capacity of shallow foundations in heterogeneous deposits using analytical and numerical methods", *Sci. Iranica. Trans. A Civ. Eng.*, **21**(3), 505.
- Jamshidi Chenari, R. and Alaie, R. (2015), "Effects of anisotropy in correlation structure on the stability of an undrained clay slope", *Georisk Assess. Manage. Risk Eng. Syst. Geohazard.*, **9**(2), 109-123.
- Jamshidi Chenari, R. and Kamyab Farahbakhsh, H. (2015), "Generating non-stationary random fields of auto-correlated, normally distributed CPT profile by matrix decomposition method", *Georisk Assess. Manage. Risk Eng. Syst. Geohazard.*, **9**(2), 96-108.
- Jamshidi Chenari, R., Ghorbani, A., Eslami, A. and Mirabbasi, F. (2018a), "Behavior of piled raft foundation on heterogeneous clay deposits using random field theory", *Civ. Eng. Infrastruct. J.*, **51**(1), 35-54.
- Jamshidi Chenari, R., Kamyab Farahbakhsh, H., Heidarie Golafzani, S. and Eslami, A. (2018b), "Non-stationary realisation of CPT data: Considering lithological and inherent heterogeneity", *Georisk Assess. Manage. Risk Eng. Syst. Geohazard.*, 1-14.
- Ji, J. and Liao, H.J. (2014), "Sensitivity-based reliability analysis of earth slopes using finite element method", *Geomech. Eng.*, **6**(6), 545-560.
- Jimenez, R. and Sitar, N. (2009), "The importance of distribution types on finite element analyses of foundation settlement", *Comput. Geotech.*, **36**(3), 474-483.
- Kasama, K. and Zen, K. (2011), *Effects of Spatial Variability of Soil Property on Slope Stability*, in *Vulnerability, Uncertainty, and Risk: Analysis, Modeling, and Management*, 691-698.
- Koumoto, T. and Houlby, G.T. (2001), "Theory and practice of the fall cone test", *Geotechnique*, **51**(8), 701-712.
- Le, T.M., Fatahi, B., Khabbaz, H. and Sun, W. (2017), "Numerical optimization applying trust-region reflective least squares algorithm with constraints to optimize the non-linear creep parameters of soft soil", *Appl. Math. Modell.*, **41**(1), 236-256.
- Fatahi, B. and Le, T.M. (2016), "Trust-region reflective optimisation to obtain soil visco-plastic properties", *Eng. Comput. Int. J. Comput.-aid. Eng. Software*, **32**(2), 410-442.
- Lim, K., Cassidy, M.J., Li, A.J. and Lyamin, A.V., (2016), "Mean parametric Monte Carlo study of fill slopes", *Int. J. Geomech.*, **17**(4), 04016105.
- Lombardi, M., Cardarilli, M. and Raspa, G. (2017), "Spatial variability analysis of soil strength to slope stability assessment", *Geomech. Eng.*, **12**(3), 483-503.
- Lu, X.L., Qian, Z.Z., Zheng, W.F. and Yang, W.Z. (2016), "Characterization and uncertainty of uplift load-displacement behaviour of belled piers", *Geomech. Eng.*, **11**(2), 211-234.
- Nguyen, L. and Fatahi, B. (2016), "Behaviour of clay treated with

- cement & fibre while capturing cementation degradation and fibre failure-C3F Model”, *Int. J. Plasticity*, **81**(1), 168-195.
- Nguyen, L., Fatahi, B. and Khabbaz, H. (2017), “Development of a constitutive model to predict the behavior of cement-treated clay during cementation degradation: C3 Model”, *Int. J. Geomech.*, **17**(7), 04017010.
- Park, J.W. and Song, J.J. (2009), “Numerical simulation of a direct shear test on a rock joint using a bonded-particle model”, *Int. J. Rock Mech. Min. Sci.*, **46**(8), 1315-1328.
- Parsa-Pajouh, A., Fatahi, B. and Khabbaz, H. (2016), “Experimental and numerical investigations to evaluate two-dimensional modeling of vertical drain-assisted preloading”, *Int. J. Geomech.*, **16**(1), B4015003.
- Popescu, R., Deodatis, G. and Nobahar, A. (2005), “Effects of random heterogeneity of soil properties on bearing capacity”, *Prob. Eng. Mech.*, **20**(4), 324-341.
- Schmertmann, J.H. and Osterberg, J.O. (1960), “An experimental study of the development of cohesion and friction with axial strain in saturated cohesive soils”, *Proceedings of the Research Conference on Shear Strength of Cohesive Soils*, Boulder, Colorado, U.S.A., June.
- Schmertmann, J.H. (1964), *Generalizing and Measuring the Hvorslev Effective Components of Resistance with Discussion*, in *Laboratory Shear Testing of Soils*, ASTM International, West Conshohocken, Pennsylvania, U.S.A.
- Shrestha, S., Ravichandran, N. and Rahbari, P. (2017), “Geotechnical design and design optimization of a pile-raft foundation for tall onshore wind turbines in multilayered clay”, *Int. J. Geomech.*, **18**(2), 04017143.
- Sridharan, A. and Nagaraj, H.B. (2005), “Plastic limit and compaction characteristics of fine grained soils”, *Proc. Inst. Civ. Eng. Ground Improv.*, **9**(1), 17-22.
- Srivastava, A. and Babu, G.S. (2011), “Deflection and buckling of buried flexible pipe-soil system in a spatially variable soil profile”, *Geomech. Eng.*, **3**(3), 169-188.
- Trauner, L., Dolinar, B. and Mišič, M. (2005), “Relationship between the undrained shear strength, water content, and mineralogical properties of fine-grained soils”, *Int. J. Geomech.*, **5**(4), 350-355.
- Vanmarcke, E.H. (1977), “Probabilistic modeling of soil profiles”, *J. Geotech. Eng. Div.*, **103**(11), 1227-1246.
- Wang, T., Zhou, G., Wang, J., Zhao, X. and Yin, L. (2018), “Stochastic analysis for uncertain deformation of foundations in permafrost regions”, *Geomech. Eng.*, **14**(6), 589-600.